Scilight

Photochemistry and Spectroscopy
https://www.sciltp.com/journals/ps

Article

The Influence of Sulphur on Anharmonic Features of Vibrational Circular Dichroism, on Electronic Circular Dichroism and on Optical Rotatory Dispersion: A Study of (*R*)-2-Chloromethyl-Oxirane, (*R*)-2-Methyl-Oxirane, (*R*)-2-Chloromethyl-Thiirane, and (*R*)-2-Methyl-Thiirane

Marco Fusè [1], Sergio Abbate [1,2], Giuseppe Mazzeo [1], Lorenzo Celio [3], Francesca Leonelli [3], Bruno Brunetti [4], Cecilia Cagliero [5], Carlo Bicchi [5], Stefano Stranges [6,7] and Giovanna Longhi [1,2,*]

[1] Dipartimento di Medicina Molecolare e Traslazionale, Università degli Studi di Brescia, Viale Europa 11, 25123 Brescia, Italy
[2] Research Unit of Brescia, Istituto Nazionale di Ottica (INO), CNR, 25123 Brescia, Italy
[3] Dipartimento di Chimica, Università "La Sapienza", 00185 Roma, Italy
[4] Istituto per lo Studio dei Materiali Nanostrutturati (ISMN), CNR, Università "La Sapienza", 00185 Roma, Italy
[5] Dipartimento di Scienza e Tecnologia del Farmaco, Università degli Studi di Torino, 00124 Torino, Italy
[6] Dipartimento di Chimica e Tecnologia del Farmaco, Università "La Sapienza", 00185 Roma, Italy
[7] Laboratorio TASC, Istituto Officina dei Materiali (IOM), Consiglio Nazionale delle Ricerche (CNR), 34149 Trieste, Italy
* Correspondence: giovanna.longhi@unibs.it; Tel.: +39-030-3717415

How To Cite: Fusè, M.; Abbate, S.; Mazzeo, G.; et al. The Influence of Sulphur on Anharmonic Features of Vibrational Circular Dichroism, on Electronic Circular Dichroism and on Optical Rotatory Dispersion: A Study of (*R*)-2-Chloromethyl-Oxirane, (*R*)-2-Methyl-Oxirane, (*R*)-2-Chloromethyl-Thiirane, and (*R*)-2-Methyl-Thiirane. *Photochemistry and Spectroscopy* **2026**, *2*(1), 9. https://doi.org/10.53941/ps.2026.100009

Received: 21 November 2025
Revised: 8 January 2026
Accepted: 9 January 2026
Published: 4 March 2026

Abstract: The vibrational circular dichroism (VCD) spectra of (*R*)-2-chloromethyl-oxirane and (*R*)-2-chloromethyl-thiirane have been recorded in a vast spectral region including mid-IR, CH-stretching fundamentals and bending-CC/CO(CS) overtone/combination regions in the mid-IR, and CH-stretching overtone/combination regions in the near infrared (NIR). The presence of sulfur is associated with intensification of the NIR-VCD spectra, similarly to what is monitored with electronic circular dichroism (ECD) and optical rotatory dispersion (ORD). DFT calculations, dealing with anharmonicity at the GVPT2 level or based on the local mode approximation, permit to correctly predict the large majority of observed VCD and IR/NIR bands and to explain the role of various molecular moieties. Also, ORD data are better interpreted by including anharmonic vibrational contributions.

Keywords: methyloxirane; methylthiirane; chloromethyl derivatives; vibrational circular dichroism (VCD); anharmonicity; GVPT2 DFT calculations; local mode calculations; optical rotatory dispersion (ORD); electronic circular dichroism (ECD)

1. Introduction

Methyl-oxirane in its chiral form has a long story in spectroscopy: indeed it aroused great interest in astrochemistry, after it had been claimed, based on microwave spectroscopy data, that it was spotted in the far universe as the first chiral molecule in space [1]. The chiral nature, racemic or with enantiomeric excess (e.e.), of the detected molecular system couldn't be determined in this discovery. Many spectroscopic studies were conducted to define chiroptical properties of methyl oxirane and its derivatives in different energy regimes. Ionizing radiation was used to characterize circular dichroism of photoelectron emission of methyl oxirane by Photo Electronic Circular Dichroism (PECD) [2–4], while at lower energies the studies involved optical rotation dispersion (OR/ORD) [5] and vibrational optical activity (VOA) [6] methods, like Raman optical activity (ROA) [7] or vibrational circular dichroism (VCD) [8]. The choice of the last three methods was preferred over standard

electronic circular dichroism (ECD), due to the absence or small intensity of ECD signals in the normally accessible UV-vis range with a couple of studies reported and carried out, below 180 nm, by the use of synchrotron radiation CD or dedicated vacuum UV (VUV)-CD spectrometers [9–11]. We contributed a bit to these studies, extending VCD investigations of methyl oxirane, in both enantiomeric forms to a wider range, including the near infrared (NIR) region and comparing with the corresponding chiroptical data of (*R*)-2-methyl thiirane [12]. For the latter compound we also measured ECD spectra at ca. 270 nm (*vide infra*).

In the present work we consider two molecules closely related to methyl oxirane and methyl thiirane, namely (*R*)-2-chloro-methyl-oxirane and (*R*)-2-chloro-methyl-thiirane, the first of which had already been studied by Wang and Polavarapu [13] and by some of us previously [14]. In this work we concentrate on the effects caused by the introduction of the sulfur atom in place of the oxygen atom, and by the substitution of the methyl group with the chloromethyl group, especially in terms of the VCD and IR/NIR intensities, rather than only of the vibrational frequencies. In Table 1, we compare the OR data at 589 nm (see also Scheme 1 for the chemical structures of the four compounds). Introduction of the sulfur atom appears to increase the magnitude of the observed OR. Also, the presence of the chlorine atom appears to give rise to some increase of OR by ca. a factor close to 2.4 for similar solvent and concentration conditions. In any case the calculation of OR values, which could help in understanding the role of sulfur with respect to oxygen, even though looks difficult [15,16], is also in part related to vibrational anharmonic aspects, as recently treated by some of us [17] and thus is relevant for the present investigation. In extending the study to the thiirane compounds, on which we had a previous experience (and this study in a way completes our previous investigations), we further prove the role of anharmonicity as essential to explain the VOA spectra in detail. However, since the ECD data for (*R*)-2-methyl-thiirane, (*R*)-2-chloro-methyl-thiirane are available and somewhat interesting, we present also them in a subsection of the "Results and Discussion" section, aiming at finding some empirical connection with ORD and VCD data.

Table 1. Specific optical rotation values $[\alpha]_D$ at 20 °C (at 589 nm) for the four molecules under study [2-Methyl-Oxirane, Chloro-2-Methyl-Oxirane, and 2-Methyl-Thiirane, 2-Chloro-Methyl-Thiirane] in (*R*) enantiomeric form: * notice the large variability of measured OR values due to solvent dependence as proven by P.H. Vaccaro et al. [15]; ** this work.

(*R*)-(–)-Me-Cl-Ox → +34° (c 1 in CCl_4) *	(*R*)-(+)-Me-Ox → +14° (c 1 in CCl_4) *
(*R*)-(+)-Me-Cl-Thii → +134° (c 1 CCl_4) **	(*R*)-(+)-Me-Thii → +56° (c 1 CCl_4) **

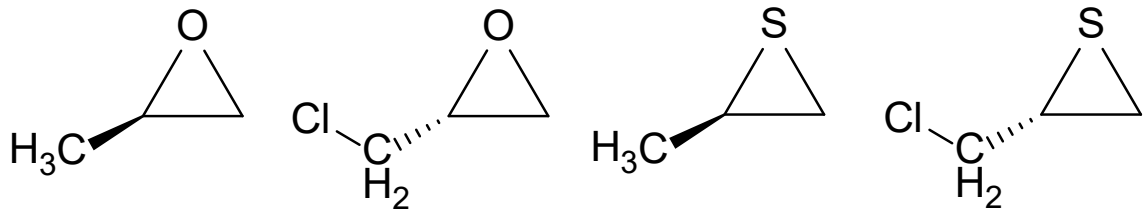

(*R*)-(+)-Me-Ox (*R*)-(–)-Me-Cl-Ox (*R*)-(+)-Me-Thii (*R*)-(+)-Me-Cl-Thii

Scheme 1. Structure of the four chiral compounds studied here: (*R*)-2-methyl-oxirane, (*R*)-2-chloromethyl-oxirane, and (*R*)-2-methyl-thiirane, (*R*)-2-chloromethyl-thiirane.

2. Materials and Methods

Below, we briefly describe how the (*R*)-2-(chloromethyl)thiirane was obtained and characterized, since this compound is not present in the literature in enantio-pure form. We conclude this section by presenting the chiroptical methods employed and the computational tools used.

2.1. Experimental Methods: Synthesis of (R)-2-(chloromethyl)thiirane and Characterization

Conversion of (*S*)-2-(chloromethyl)oxirane to (*R*)-2-(chloromethyl)thiirane was performed in water according to a known procedure, which had been applied in this context, with ammonium thiocyanate at room temperature (20 °C). This synthetic route was selected, among those reported in the literature [12,18,19], because it involves a S_N2 mechanism that prevents the racemization of the chiral centre, according to Scheme 2.

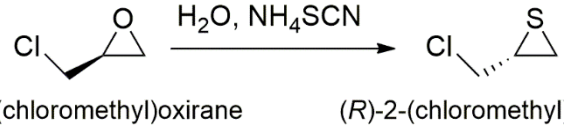

(*S*)-2-(chloromethyl)oxirane (*R*)-2-(chloromethyl)thiirane

Scheme 2. Preparation of (*R*)-2-(chloromethyl)thiirane from (*S*)-2-(chloromethyl)oxirane in H_2O at 20 °C with ammonium thiocyanate.

The synthesized 2-(chloromethyl)thiirane was purified with difficulty. Indeed, the final product degraded very easily and was extremely volatile. Particularly, distillation of the reaction mixture by sample warming caused very low yields. Higher yields were only achieved by separation processes based on vacuum distillation in a low impedance transfer line between cold traps, whose temperature was controlled by thermostatic baths. The difference in vapor pressure, as a function of temperature, of solvents and the synthetized compound allowed clean extraction of 2-(chloromethyl)thiirane. In this procedure, monitoring of the nature of the extracted vapor in the transferred line, accomplished by recording He Iα (21.218 eV) photoelectron spectra (PES), was crucial. The vapor pressure is 0.13 atm at 70–72 °C, while the normal boiling point is not known since the pure compound decomposes, likely forming a solid polymer, at high temperature.

22.5 g of (*S*)-2-(chloromethyl)oxirane (0.24 mol, 19 mL), as purchased by Merck Life Science (98% purity), were introduced in a round-bottom flask with 495 mL distilled water and 112.5 g of ammonium thiocyanate (1.5 mol). The solution was magnetically stirred at 20 °C for four hours, then 120 mL of pentane were added to quench the reaction. The solution was debated in an extraction funnel to separate the organic phase, containing the synthesized compound, from the aqueous solution. The 120 mL pentane extraction from the aqueous solution was repeated twice. The organic phase, collecting the three extracted fractions, was dried over anhydrous Na_2SO_4. The solution thus obtained was filtrated and placed in a 500 mL two-necked flask that was connected to the vacuum transfer line.

Pentane and other volatile species (atmospheric gases) were removed from the liquid solution, kept at –30 °C, in the transfer line by rough pumping with a mechanical rotary pump for 15 h. A further 5-h pumping, while gradually increasing the temperature to –10 °C, was needed to remove completely pentane from the solution containing the synthetized thiirane. (*R*)-2-(chloromethyl)thiirane was extracted as pure compound from the solution kept at +5 °C by transferring, in static vacuum, into a 50 mL flask, which was dipped in liquid nitrogen. 75 h were needed for a complete extraction of the synthetized thiirane.

Pure (*R*)-2-(chloromethyl)thiirane was obtained with 16% yield. Chemical purity of the methylthiirane was checked by: (i) ^{1}H-NMR (400.13 MHz, C6D6): δ 1.59 (1H, dd of CH2), 1.88 (1H, dt of CH2), 2.57 (1H, m, CH), 2.66 (1H, dd of CH2Cl), 3.27 (1H, ddd of CH2Cl) (see Figure S1); and by (ii) ^{13}C-NMR (100.61 MHz, C6D6): 48.7, 33.5, 25.3 (see Figure S2).

Mass-Spectrometric methods were also employed to further check enantiomeric purity (see Figure S3 and related text). Finally optical rotation (OR) was measured through a polarimeter measurement with a Jasco P2000 Polarimeter, yielding $[\alpha]_D$ = +134.4 at 20 °C (Table 1). Optical rotatory dispersion (ORD) curves were also built by linearly connecting measure OR values from 589 to 405 nm (*vide infra*).

2.2. Experimental Methods: Chiroptical Spectroscopies.

We measured ORD with a Jasco P2000 polarimeter with the sample solution contained in the quartz cylindrical 10 cm cuvette normally employed for OR measurements; the dedicated software allowed to derive specific optical rotation values for all considered wavelengths and an ORD curve is drawn by linearly connecting the measured OR values: we notice that for (*R*)-2-chloromethyl-thiirane the ORD curve rapidly increases, suggesting an anomalous trend starting at ca. 380 nm, and we think that this behavior is determined by the close-by ECD Cotton positive band observed at 270 nm (*vide infra*). The behavior of ORD for (*R*)-2-methyl-thiirane is even odder and will be discussed later.

For ECD measurements we used a Jasco 815SE apparatus with samples contained in a 0.1 mm cuvette for (*R*)-2-(methyl)thiirane and (*R*)-2-(chloromethyl)thiirane in C_6H_{12} at the low concentration values $5.3\cdot10^{-3}$ M and $9.0\cdot10^{-3}$ M respectively, to broaden the range the range as much as possible (*vide infra*). 10 accumulations were taken, and solvent ECD spectra recorded in the same conditions were subtracted. ECD measurements were repeated also in CCl_4 (data not reported) in order to check differences and to be coherent with IR-VCD results.

VCD spectra were recorded with a Jasco FVS 6000 FTIR instrument in the mid-IR (from 850 cm^{-1} to 2000 cm^{-1}; mid-IR + combination region) employing a MCT detector with BaF_2 cells of 0.100 mm for the region 850–1600 wavenumber and 0.500 mm for the region 1700–2200 wavenumber. 6000 scans were taken and accumulated. The same Jasco FVS 6000 FTIR instrument was employed for the fundamental CH-stretching region using quartz

cuvettes 1mm long and with an InSb detector (6000 scans). In all cases, the VCD and IR spectra of the solvent (CCl_4) were taken in the same condition and were subtracted out of the VCD and IR spectra of the solutions. When necessary, namely for the mid-IR 2/3 quanta overtone and combination region, also the VCD and IR spectra of (*R*)- and (*S*)-2-(chloromethyl)oxirane were re-measured or measured *de novo* with the same protocol of the adjacent region and as done before by us.

In the NIR regions (from 2000 to 1000 nm namely in the 5000–9000 cm^{-1} range) VCD spectra were taken with a home-made dispersive instrument previously described [20], encompassing the $\Delta v = 2$ CH-stretching first overtone region, the combination of $\Delta v = 2$ CH-stretching transition and $\Delta v = 1$ HCH-bending transitions (which we call $\Delta v = 2.5$ region), and the $\Delta v = 3$ CH-stretching second overtone region. Except for (*R*)-2-chloro-methyl-oxirane $\Delta v = 2$ measurements, which were performed on 1 M/CCl_4 solutions contained in a 10 mm quartz cuvette, all NIR-VCD measurements were recorded on neat samples contained in quartz cuvettes of different path-length (1 mm for $\Delta v = 2$ and 5 mm for the others regions). At least 4 scans were taken, as well as the so-called ABL spectra were recorded and subtracted from VCD spectra.

2.3. Computational Methods

The Gaussian16 package [21] was employed to calculate the VCD, ECD spectra, the corresponding absorption spectra, and frequency-dependent optical rotation. When necessary, GVPT2 approach was followed as it appears in Gaussian16, to evaluate the anharmonic features in either the absence or the presence of Darling-Dennison or Fermi resonance effects between overtones/combination transitions and fundamentals. Up to 3-quanta transitions were considered [22], as done in our previous works [12]. (In Figure S8 comparison of harmonic and anharmonic results is reported for (*R*)-chloromethyl-thiirane and (*R*)-chloromethyl-oxirane. Also an input example for the procedure is reported). The conformational search was first run, by acting directly on just the one degree of conformational freedom which we assumed responsible for molecular conformations, namely the dihedral angle Cl-C-C-O(S). The three conformers thus found, after minimization at the DFT level, are presented in Figure 1 and are named as Gauche I, Gauche II and Cis, according to Wang and Polavarapu [13], and Durig et al. [23,24] looking at the values of the dihedral angle γ formed by the C–Cl bond and the bisector of the ring. The computational level was B3PW91/jun-cc-pVTZ and results compared well with our previous investigation of (*R*)-2-chloromethyl-oxirane, which had been conducted at the B3LYP/6-311G(2d,2p) level. Simulating spectroscopic properties, both the gas-phase condition and the PCM method for CCl_4 were considered. Since they did not exhibit large differences, with the only exception of OR data, we present here the gas-phase case. A recent in-depth study of the conformational properties for chloromethyl-oxirane and chloromethyl-thiirane has been published [25] and conclusions are similar to the ones proposed here (see Table S1) as well as our previous study [14]. Consequently, we adopted the Boltzmann factors reported in [25] for CCl_4 and neat liquids. (In Table S1 energy values and Boltzmann factors are reported, in Table S2 geometry parameter obtained after optimization). For the NIR and fundamental CH-stretching region also the local mode approach was pursued, which is presented below just for the CH-stretching cases. Local mode calculations were performed with lcmodslib set of python scripts [26] which prepares and processes Gaussian files.

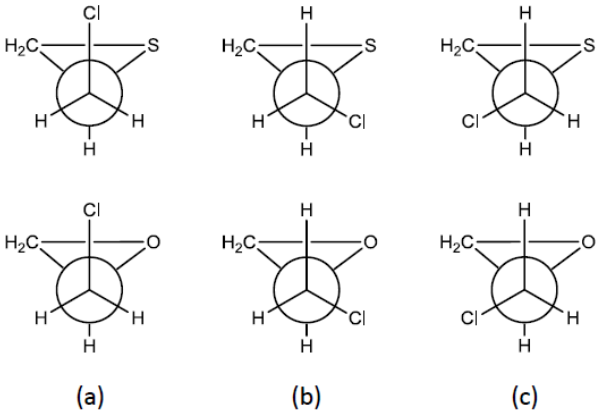

Figure 1. Schematic representation of the Cis (**a**); Gauche I (**b**) and Gauche II (**c**) conformers of (*R*)-chloromethyl thiirane (top) and of (*R*)-chloromethyl oxirane (bottom). Notation taken from ref. [13]. (Boltzmann) population factors (γ values in parenthesis are for the dihedral angle between CCl and bisector line of S(O)-CH_2 bond) for (*R*)-chloromethyl thiirane: (**a**) 2% ($\gamma \approx 8°$); (**b**) 16% ($\gamma \approx -118°$); (**c**) 82% ($\gamma \approx +123°$); for (*R*)-chloromethyl oxirane: (**a**) 8% ($\gamma \approx 15°$); (**b**) 34% ($\gamma \approx -117°$); (**c**) 58% ($\gamma \approx +127°$). Populations given for CCl_4 solutions [25].

For calculated IR and VCD spectra different bandwidths were adopted, depending on the spectroscopic region: 7 cm^{-1} in the 850–2400 cm^{-1} range; 10 cm^{-1} in 2750–3200 cm^{-1} range; 15 cm^{-1} for $\Delta v = 2$ and 30 cm^{-1} for $\Delta v = 2.5$ and $\Delta v = 3$. For ECD spectra, 0.15 eV bandwidth was applied and no shift in energy was adopted.

3. Results and Discussion

3.1. VCD

In Figure 2 we report for an overall comparison the experimental VCD and IR spectra in all the investigated regions. We can make the following empirical observations on the VCD/IR data. (1) The presence of the chlorine atom in the chloro-methyl group assigns to the latter a larger Cahn-Ingold-Prelog [27] (CIP) priority than the nearby –($CO(S)H_2$) group, while the methyl group has a smaller priority index than –($CO(S)H_2$) (see Scheme 1): this explains some interesting sign differences in (*R*)-2-chloro-methyl-oxirane with respect to (*R*)-2-methyl-oxirane and in (*R*)-2-chloro-methyl-thiirane with respect to (*R*)-2-methyl-thiirane. This is particularly evident in the high overtone/local mode region; (2) the substitution of O with S appears to increase VCD intensities (and also absorption intensities) in the overtone $\Delta v = 3$, where the local mode behavior dominates; (3) the mid-IR and, to a lesser extent, the CH-stretching fundamentals for the chloromethyl compounds appear less intense in VCD than the corresponding methyl compounds: one cause for this might be that three different inequivalent conformers of the chloromethyl group are expected, while the methyl group is freely rotating.

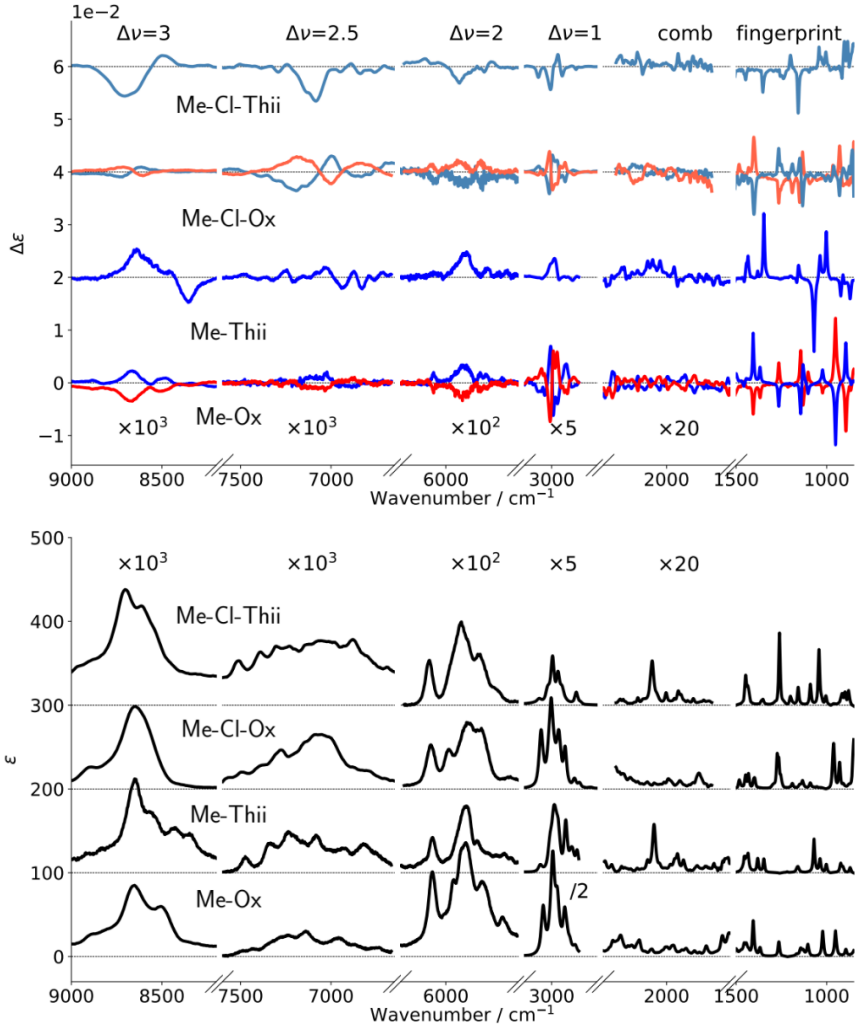

Figure 2. Comparison of experimental VCD (top) and IR (bottom) spectra for (*R*)-chloromethyl thiirane, (*R*)- and (*S*)-chloromethyl oxirane, (*R*)-methyl thiirane and (*R*)- and (*S*)-methyl oxirane (blue lines are used for the *R* configuration and red ones for the *S* configuration) from 900 to 9000 cm^{-1}. Vertical axis is in intensity units: ($M^{-1}cm^{-1}$) ≡ ($10^3 cm^2/mol$) for the fingerprint region (900–1500 cm^{-1}); for the other regions data need to be multiplied by the indicated factors, since units are correspondingly smaller. See the experimental section for details. (Please notice the intensity factor e − x = 10^{-x} for VCD y-scale, given on top of the VCD spectra).

Let us now examine if calculations back up these observations. From here, in the text, we limit ourselves to the two chloromethyl molecules of the title for VCD/IR(NIR), since comparison of methyl oxirane and methyl thiirane data and anharmonic calculations were presented and amply commented in ref. [12].

3.1.1. VCD in the Mid-IR

In Figure 3 we report the comparison of experimental and calculated IR and VCD spectra for (*R*)-2-chloromethyl-oxirane and (*R*)-2-chloromethyl-thiirane in the standard mid-IR and in the less standard region between 1800 and 2100 cm^{-1}. The former region is determined mostly by fundamental bending and CC/CO(CS) stretching transitions, while the latter contains just combination and overtone transitions, whose fundamentals are located at ca. 1000 cm^{-1}. The experimental data are all from our lab, and calculations include anharmonicity treated at GVPT2 level as implemented in Gaussian [12,21], we wish to remind that, because of anharmonicity treating, no scaling factor was necessary. The computational results are Boltzmann averages over the spectra of the three conformers; the results for the single conformers are given in Figure S4A,B and one can see that the three conformers do not give very different results in sign and magnitude (the Cis conformer contributing very little, being weakly populated), in contrast to what happens in the CH-stretching region. As observed by Palumbo et al. [25] and by Durig et al. [23,24], the Gauche II conformer, exhibiting small permanent dipole moment, largely prevails in CCl_4 solvent, as well as in all apolar solvents and in the gas phase. In the condensed phase the polar Gauche I acquires importance, which should be kept in mind when analyzing neat liquid data. Computational results in the standard mid-IR region are pretty good for all IR/VCD bands and several features are common to both compounds with higher intensity in the oxirane case (see for example the CH_2-bending band at 1405 cm^{-1}). Compared with our previous investigations of (*R*)-2-methyl-oxirane and (*R*)-2-methyl-thiirane, (*R*)-2-chloromethyl-oxirane and (*R*)-2-chloromethyl-thiirane exhibit an extra intense IR absorption band at ~1250 cm^{-1} with corresponding little VCD for (*R*)-2-chloromethyl-thiirane and medium VCD for (*R*)-2-chloromethyl-oxirane. This is due to CH_2 wagging in the CH_2Cl group, which implies strong dipole moment derivative and thus high IR intensity, but is sufficiently removed from the stereogenic carbon, thus causing non-large VCD. Also the combination/overtone region is reproduced pretty well by calculations, which witnesses the reliability and power of the GVPT2 routine in Gaussian16; though non trivial, this result is not fully unexpected, based on two previous results from our group [12,28] but also on the fact that in these regions the role of resonances is not as crucial as in the next CH-stretching ones. Besides, a noteworthy similarity between the present chlorinated cases and the other previously studied non-chlorinated cases is noticed for the combination band region, which does not involve the chlorine atom vibrational motion.

In coming now to conclusions on the role played by the sulfur atom S with respect to the oxygen O in this region, based on the results of Figure 3 and on the previous results for (*R*)-2-methyl-oxirane and for (*R*)-2-methyl-thiirane, we may state that the main differences between S-cases and O-cases are found at about 1150 cm^{-1} and in the IR absorption band at ca. 2100 cm^{-1}; these bands correspond to the fundamental and the first overtone of the CH_2 wagging on the thiirane ring, respectively, while the analogous overtone wagging for methyl-oxirane and chloromethyl-oxirane is found at higher energy, about 2270 cm^{-1}. In any case, for both thiirane compounds, the combination region shows sharp bands and VCD features with large dissymmetry ratio. In contrast, the corresponding signal in (*R*)-2-chloromethyl oxirane shows only medium intensity broad features. Overall, the DFT anharmonic calculations reproduce experimental data in frequencies, signs (for VCD) and VCD/IR intensities (especially for the thiirane derivative).

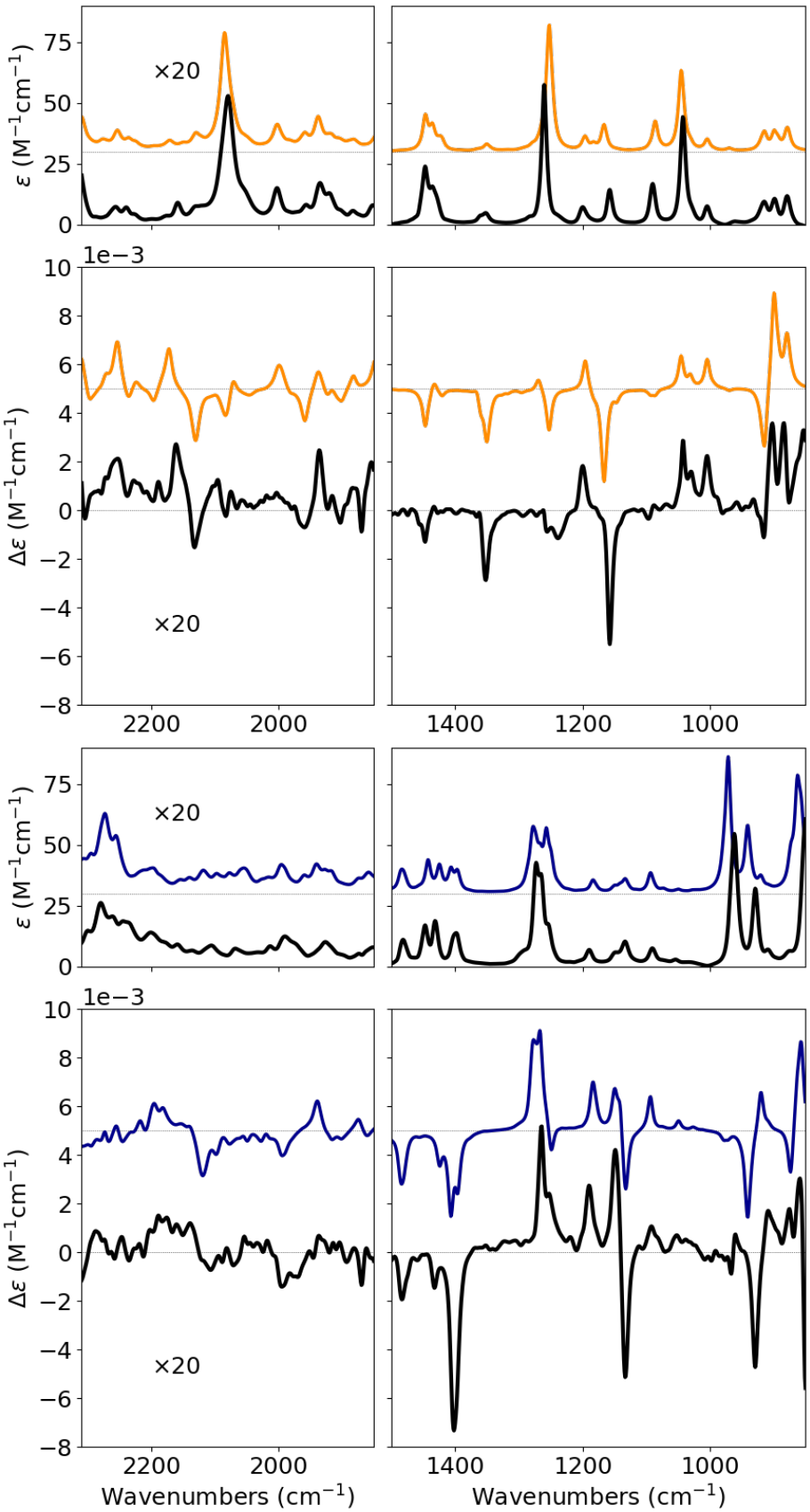

Figure 3. Comparison of experimental IR and VCD spectra with corresponding computed spectra for (*R*)-chloromethyl thiirane (top two panels) and (*R*)-chloromethyl oxirane (bottom two panels) for the fingerprint and lower combination data based on GVPT2 approach. All experimental spectra are in black, computed spectra for (*R*)-chloromethyl thiirane are orange, computed spectra for (*R*)-chloromethyl oxirane are blue. Y-axes units are with no multiplication factor for the fingerprint region; for the combination region, spectra need to be divided by the indicated ×20 factor. (Please notice the intensity factor e − x = 10^{-x} for VCD y-scale, given above the VCD spectra).

3.1.2. VCD in the Fundamental and Overtone Regions of CH-Stretching

Results for VCD and IR/NIR absorption spectra of the CH-stretching regions (the Δv = 1 fundamental and the Δv = 2 and Δv = 3 overtones) are given in Figure 4, obtained through the GVPT2 approach and are superimposed to the results from the local mode (LM) approach: in both cases they are Boltzmann averages of conformer calculated spectra weighed with the population factors given in the caption of Figure 1, and are also superimposed to experimental results, for sake of comparison. Results for each conformer (Gauche II, Gauche I and Cis) are given in Figure S4C for the GVPT2 approach and in Figure S5B,C for the local mode case, with indication of contributions of each CH local mode (please consider Figure S5A for the definition of bonds). The CH-stretching regions of (*R*)-2-chloro-methyl-oxirane and (*R*)-2-chloro-methyl-thiirane exhibit conformer dependence, as already recognized for the former molecule [14]. This comes about since the three conformers bear contributions of different signs, while in the mid-IR differences were not so evident; this has an higher influence for (R)-2-chloromethyl-oxirane due to more similar Boltzmann factors values for the Gauche I and Gauche II cases. However still the Gauche II conformer is the one exhibiting the best results as compared to experiment, in accord with the conclusions of Durig et al. [23,24] and of Palumbo et al. [25].

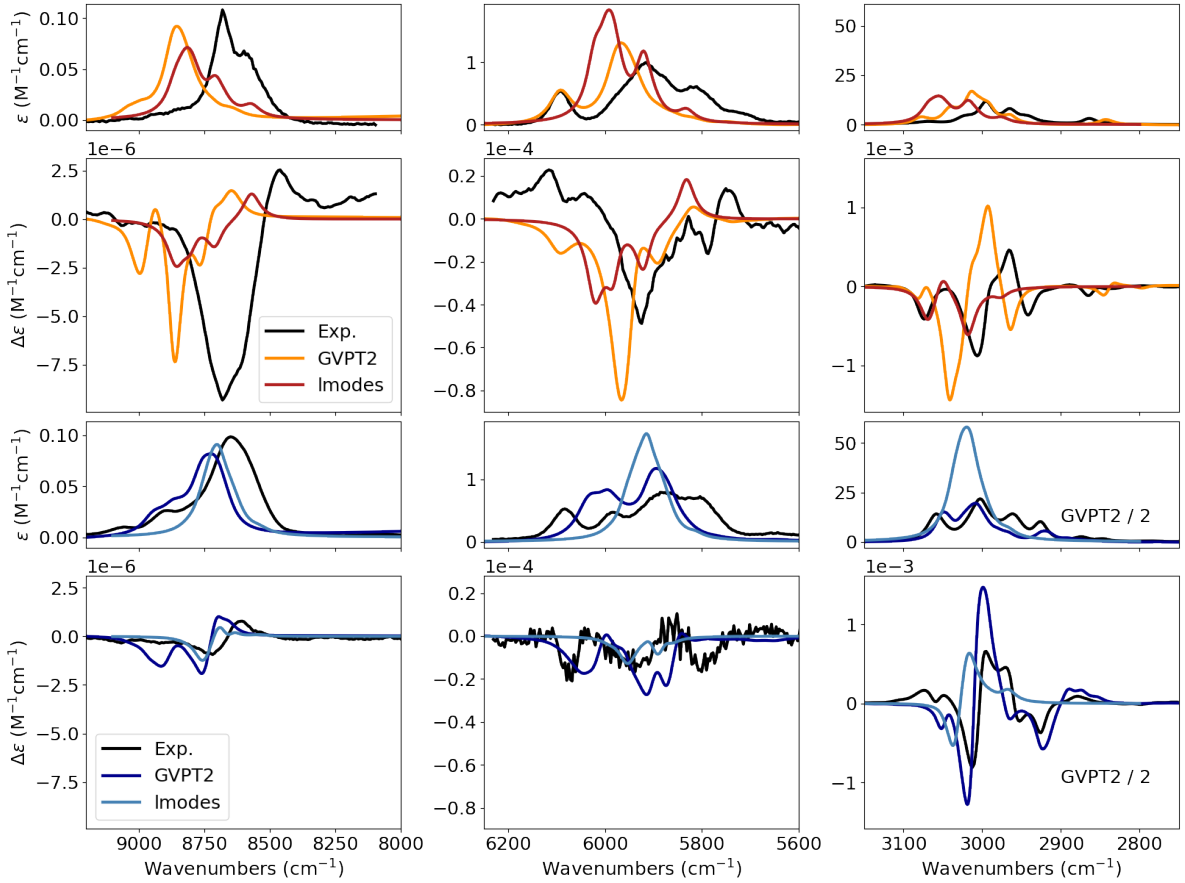

Figure 4. Comparison of experimental IR/NIR and VCD spectra with corresponding computed spectra for (*R*)-chloromethyl thiirane (top two panel rows) and (*R*)-chloromethyl oxirane (bottom two panel rows) for the fundamental (Δv = 1, right), first overtone (Δv = 2, center) and second overtone (Δv = 3, left) (compare with Figure 2) based on GVPT2 approach and local mode approximation. All experimental spectra are in black, computed spectra for (*R*)-chloromethyl thiirane are orange (GVPT2) or red (local mode), computed spectra for (*R*)-chloromethyl oxirane are either dark blue (GVPT2) or light blue (local mode). Boltzmann factors to best represent the experimental conditions (CCl_4 solution and neat) were used to obtain the average spectra. (Please notice the intensity factor e − x = 10^{-x} for VCD y-scale, given above the VCD spectra).

As a first general comment, it becomes evident that, for increasing Δv, either the ω_0 value in the Birge-Sponer expansion [12,14] is calculated a bit too large or the χ value is calculated a bit too small in both our approaches (GVPT2 and LM). As previously noted, this might be reconciled by perturbing the systems along internal coordinates [29,30]. Secondly, the GVPT2 approach, being based on a normal mode zero-order Hamiltonian, is superior to the LM approach for absorption spectra at Δv = 1, while the two approaches give similar results for Δv = 3; surprisingly the LM method gives good results for VCD at Δv = 1 and Δv = 2, which are the normal mode

region and the transitional region from the normal to the local mode regime respectively [31]. As described in Figure S5B,C, the LM approach permits one to appreciate that the CH local oscillators behave differently in the three conformers at each Δv transition and not only for the CHs in the chloromethyl moiety, but also in the epoxy/episulfide ring. Yet, for the major Gauche II conformer (as well as for Gauche I) one may notice that the C_2-H_3 (see Figure S5A–C) local mode gives a positive VCD band, while C_2–H_4 and C_5–H_6 local modes give two negative VCD bands and the three signals dominate the VCD spectra at Δv = 3. A similar pattern is observed, obviously and concurrently with the change in C.P.I. priorities, in the non-chlorinated chiral (*R*)-2-methyl-oxirane and (*R*)-2-methyl-thiirane (see the Supplementary of Fusè et al. [12]). This is particularly evident in the presence of the S atom. Some further help in understanding the behavior of the different local modes comes from Figure S6A,B, providing the graphs of APT (atomic polar tensor) and AAT (atomic axial tensor) components of all H-atoms as functions of the corresponding CH-stretching coordinates and in the summarizing Figure S7 for the values of APT/AAT and their first derivatives with respect to CH bond lengths at equilibrium. It is interesting to note, in this respect, that in the sulfur cases (i.e., both for methyl-thiirane and chloromethyl-thiirane) the component of the electric dipole $\partial\mu_z/\partial z$ along the CH bond, expected to give the main contribution to the dipole strength for fundamentals, presents a lower value than the oxygen analogous, and indeed the observed absorption spectra for Δv = 1 are weak. At the same time, the sulfur molecules exhibit high values for the magnetic anharmonic terms transverse to the CH bond directions (Figure S7) which fact can justify the observed VCD activity at Δv = 2 and 3, higher for thiirane compounds than for oxirane compounds. The three ring CH bonds interact (possibly via a polarizability mechanism [32]) with the HOMO orbital (see Figures S5A), which has strong non-bonding *n* character, providing increase in the calculated intensities for the CH bond-stretchings close to the sulfur (or to the oxygen). This is reminiscent of what happens in limonene for pseudo-axial and pseudo-equatorial CHs in the vicinity of the ring double bond [28]. Somewhat similar considerations had been put forward long ago in the interpretation of ECD spectra of (*R*)-2-methyl-thiirane [33]. This evidences the diastereotopic property of axial and equatorial CH bonds as well as of the lobes of sulfur and oxygen lone pairs.

3.2. ECD and ORD for (R)-2-Methyl-Thiirane, (R)-2-Chloromethyl-Thiirane.

For sake of completeness, we report in Figure 5 the superimposed experimental and calculated ECD spectra (left) and the experimental and calculated ORD curves (center and right respectively) for (*R*)-2-methyl-thiirane (top) and for (*R*)-2-chloro-methyl-thiirane (bottom). The first ECD spectrum of methyl-thiirane was recorded by Gottarelli et al. in 1973 [33,34], the same school discussed the optical activity of the 260 nm transition of other chiral thiiranes in terms of molecular orbitals calculations attributing the band to ($n \rightarrow \sigma^*$) transition, being σ* C-S antibonding orbital. For both compounds the ECD longest wavelength band is centered at ca. 268 nm and is negative for (*R*)-2-methyl-thiirane and is positive and at 265 nm for (*R*)-2-chloro-methyl-thiirane. Once and again the sign difference reflects the change in group priorities in the application of the C.I.P. rule [27] namely, together with the Δv = 3 NIR-VCD sign, the sign of the ECD band at 268 (or 265 nm) correlates with group spatial orientation at the stereogenic carbon atom (see also references [11,14]). The main contribution to the band is the ($n \rightarrow \sigma^*$) transition, which has zero rotational strength in a symmetric context but acquires rotational strength in a dissymmetric context, according to the definition of inherently symmetric chromophore [35]. We ran our ORD measurements for three different concentration values, while ECD was measured in diluted cyclohexane solution to cover the maximum accessible wavelength range to our instrument. The measured experimental values of the g factors of the lowest energy band are rather large ($-2.78\cdot10^{-2}$ for (*R*)-2-methyl-thiirane and $3.92\cdot10^{-2}$ for (*R*)-2-chloromethyl-thiirane), being slightly larger in magnitude than twice the fine-structure constant (which is the upper bound value expected for electric-dipole allowed transitions) [36]. Due to the weak absorption band, we are in presence of a prevalently magnetic dipole allowed transition band. Similar considerations were put forward by Rodger et al. [11] based on the octant rule, and by Bendazzoli et al. [33].

The ORD curves of (*R*)-2-methyl-thiirane and (*R*)-2-chloro-methyl-thiirane at three different concentrations (to cover comparison with ECD and VCD results) are also given in Figure 5 (central panels). Both bear normal ORD dispersion increasing positive trends, with some little yet important anomalies toward small wavelengths for (*R*)-2-methyl-thiirane. Interestingly, the negative sign of the first observed ECD band for (*R*)-2-methylthiirane is in contrast with the observed increasing positive trend of ORD. Crawford et al. indeed had talked about "the difficult case of (*R*)-2-methylthiirane" [16]. According to the Kramers-Kronig relation (KK) [37–41], discontinuities in ORD are expected in presence of electronic transitions. In this case, the negative ECD transition requires the $-\infty \rightarrow +\infty$ discontinuity at ~270 nm going toward increasing energy, which seems at odds with the experimental observations. Although 270 nm lies beyond the measurable range of our polarimeter, the start of a decreasing trend is noticed at short wavelengths, i.e., between the two OR values measured at lowest wavelengths

(405 and 365 nm, see Figure 5). This agrees with the negative ECD band observed at 268 nm. In any case it is well known that ORD is determined by the superposition of contributions from different ECD rotational strengths, such that rotational strength of high energy transitions may provide more important contributions. On the contrary, the relation between experimental ECD and ORD is monotonically increasing, as expected for (*R*)-2-chloromethyl-thiirane. The full interpretation of the ORD curves is provided by DFT calculations, with explicit account for vibrational contributions, which require anharmonicity to be evaluated [17,42–45]. In facts, looking at the calculated ORD curve for (*R*)-2-methyl-thiirane (top right panel) one sees that adding vibrational contributions to the electronic effects, one better accounts for the correct ORD trend and provides larger OR values closer to experimental values. Again, this addresses the importance of the correct determination of vibrational terms. Such a problem is not manifested in (*R*)-2-chloro-methyl-thiirane, where the electronic effects overwhelm vibrational contributions and ORD is of the same sign as the observed ECD positive band. Either calculation, with or without vibrational contribution is equally good.

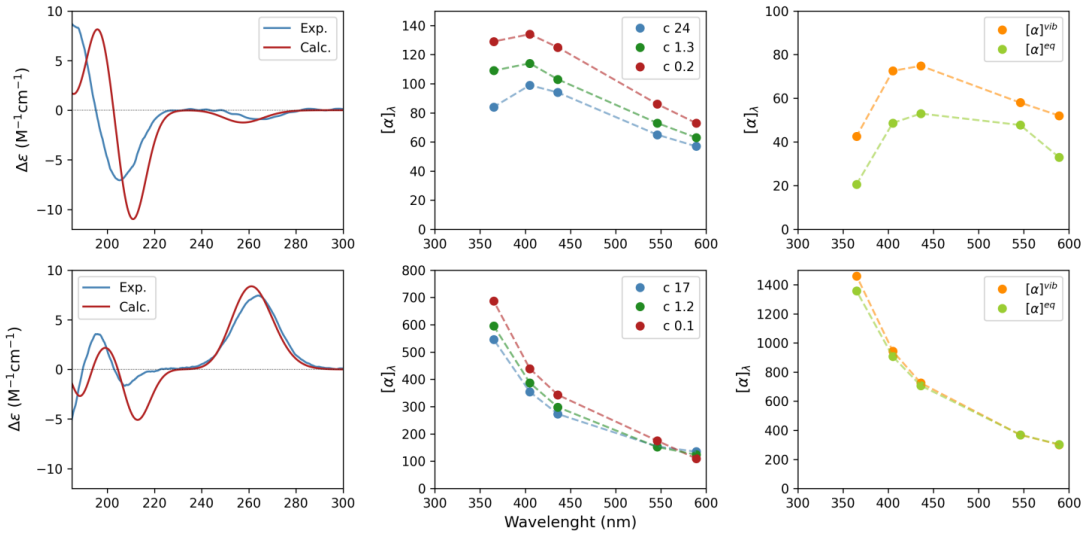

Figure 5. Experimental and calculated ORD curves (center and right respectively) and ECD spectra (left, experimental and calculated superimposed) for (*R*)-2-methyl-thiirane (top) and for (*R*)-2-chloro-methyl-thiirane (bottom). Experimental ORD curves are obtained by linearly connecting specific OR values measured at 25 °C and for the specified concentration values (g/100 mL) on CCl_4 solutions (in molarities 3.2 M, 0.18 M and 0.027 M respectively for the (*R*)-2-methyl-thirane case and 2.3 M, 0.17 M and 0.013 M for (*R*)-2-chloromethyl-thirane). ECD spectra (cyclohexane dilute solutions (~10^{-3} M), precise concentration values given in the Experimental section) are in Δε units ($M^{-1}cm^{-1} \equiv 10^3 cm^2/mol$) versus λ(nm). On the right simulated OR values at different wavelength, both the equilibrium values ($[\alpha]^{eq}$) and the vibrational corrected ones ($[\alpha]^{vib}$ at 25 °C) are reported.

4. Conclusions

In this work we have recorded and interpreted the VCD spectra of (*R*)-2-chloromethyl-oxirane and (*R*)-2-chloromethyl-thiirane; we have also discussed the comparison to the analogous spectra obtained in our previous study for (*R*)-2-methyl-oxirane and (*R*)-2-methyl-thiirane [12]. By DFT calculation, treating anharmonicity at the GVPT2 level or based on the local mode approximation, we have been able to quantitatively predict most of the observed VCD and IR/NIR bands and also to explain the role of various molecular moieties. Experiments and computational interpretation regarded a rather thorough spectral region, which includes mid-IR, CH-stretching fundamentals and bending-CC/CO(CS) overtone/combination regions in the mid-IR and CH-stretching overtone/combination regions in the near infrared (NIR).

The spectroscopic results obtained on such simple molecules, elucidates the role of sulfur in determining spectroscopic responses. The importance of sulfur in mid-IR VCD spectra in several instances and several molecular moieties was previously addressed [46–49], but, to the best of our knowledge, never in NIR-VCD spectra. In this spectra we evidenced that the presence of sulfur leads to intensification of the signals acting in particular on the anharmonic terms of the magnetic dipole transition moments. The influence of sulfur can be monitored also via electronic circular dichroism (ECD) and optical rotatory dispersion (ORD). In the Results and Discussion section the different kinds of information provided by VCD in the NIR and in the mid-IR and by ORD and by ECD are evidenced. Particularly, it is found that two good parameters for easy assignment of the absolute

configuration of (*R*)-2-methyl-thiirane and (*R*)-2-chloromethyl-thiirane are the signs of the alternating bands in Δv = 3 NIR/VCD spectra and the sign of the ECD band at ca. ~270 nm. These two types of data are opposite in the two molecules and thus they both monitor the change in priorities for the application of the CIP (Cahn-Ingold-Prelog) rule [27], despite the fact that the band is weak. Other substituted cases were presented by Moretti et al. [50], all bearing the same correlation. The ORD curves, particularly the anomalous one for (*R*)-2-methyl-thiirane, are well interpreted, if one includes the contribution of zero-point vibrational modes, which in turn are accounted by anharmonic terms [42].

Supplementary Materials

The additional data and information can be downloaded at: https://media.sciltp.com/articles/others/2603041556540082/PS-25110129-SM.pdf. Figures S1: ^{1}H-NMR (C_6D_6, 400.13 MHz) spectrum of the synthetized (*R*)-2-(chloromethyl)thiirane. Figures S2: ^{13}C-NMR (C_6D_6, 100.61 MHz) spectrum of the synthetized (*R*)-2-(chloromethyl)thiirane. Figures S3: GC-FID chromatograms of 2-(chloromethyl)thiirane samples: (a) racemic sample (red curve); (b) synthetized (*R*)-2-(chloromethyl)thiirane (black curve). Both chromatograms were obtained with the same column and experimental conditions. Figures S4: (A). Fingerprint region between 850 and 1500 cm^{-1}. Comparison of experimental IR (top) and VCD spectra (bottom) with corresponding computed spectra for all conformers and Boltzmann average (dashed lines) of (*R*)-chloromethyl thiirane (left two panels) and (*R*)-chloromethyl oxirane (right two panels) based on GVPT2 approach. All experimental spectra are in black, computed spectra for (*R*)-chloromethyl thiirane have orange-hue, computed spectra for (*R*)-chloromethyl oxirane have blue-hue. Conformer spectra were multiplied by their Boltzmann factors in CCl_4. (B). Combination/overtone region between 1850 and 2350 cm^{-1}. Comparison of experimental IR (top) and VCD spectra (bottom) with corresponding computed spectra for all three conformers (solid lines) and for the Boltzmann averages (dashed-dotted lines) of (*R*)-chloromethyl thiirane (right two panels) and (*R*)-chloromethyl oxirane (left two panels) based on GVPT2 approach. All experimental spectra are in black, computed spectra for (*R*)-chloromethyl thiirane have orange-hue, computed spectra for (*R*)-chloromethyl oxirane have blue-hue. Conformer spectra are reported as already multiplied by their Boltzmann factors calculated for CCl_4 solution. **(C).** Comparison of experimental IR/NIR (1st and 3rd from top) and VCD spectra (2nd and 4th from top) with corresponding computed spectra for all three conformers (solid lines) and for the Boltzmann averages (dotted lines) for (*R*)-chloromethyl thiirane (top two panels) and (*R*)-chloromethyl oxirane (bottom two panels) for the fundamental (Δv = 1, right), first overtone (Δv = 2, center) and second overtone (Δv = 3, left) based on GVPT2 approach. All experimental spectra are in black, computed spectra for (*R*)-chloromethyl thiirane have orange-hue, computed spectra for (*R*)-chloromethyl oxirane have blue-hue. See Figure S4A for the definition of the color coding. Conformer spectra are reported as already multiplied by their Boltzmann factors for CCl_4 solution (Δv = 1) and for the neat, (Δv = 2 and Δv = 3), the factors being taken from Palumbo et al. (Spectrochim. Acta. A. Mol. Biomol. Spectrosc. 2021, 247, 119061). In the case of (*R*)-chloromethyl oxirane in the Δv = 2 region, also the computed Boltzmann average spectrum with weights for the CCl_4 solution is reported as dashed-dotted. Figures S5: (A): Atom numbering used in calculation for (*R*)-2chloromethyl thiirane and (*R*)-2-chloromethyl oxirane. This figure may help the reader better understand the next local mode (lm) calculations; center: HOMO representation for (*R*)-2chloromethyl thiirane; right: HOMO representation for (*R*)-2chloromethyl oxirane. (The same parameters for the orbital representation used in the two cases.). (**B**): (*R*)-2-chloromethyl-oxirane. Comparison of experimental (black) and computed (blue) absorption (top row) and VCD (bottom row) spectra. TOP: calculations for the major populated Gauche II conformer. MIDDLE: calculations for the second major populated Gauche I conformer. BOTTOM: calculations for the minor populated Cis conformer. We also give as bars the contributions of each local mode to the spectra. (For the nomenclature of local modes see Figure S5A above). (**C**): (*R*)-2-chloromethyl-thiirane. Comparison of experimental (black) and computed (blue) absorption (top row) and VCD (bottom row) spectra. TOP: calculations for the major populated Gauche II conformer. MIDDLE: calculations for the second major populated Gauche I conformer. BOTTOM: calculations for the minor populated Cis conformer. We also give as bars the contributions of each local mode to the spectra. (For the nomenclature of local modes see Figure S5A above). Figures S6: (A): (*S*)-2-chloromethyl-oxirane. Dependence of the longitudinal and transverse components of the APTs and AATs for the Hydrogen atoms with respect to the CH-bond length (z-direction) (see [12] for the definition of (x,y,z) axes for the CH-bonds). APTs are in atomic unit of charge *e* (electrons), AATs are in units of (ea_0)/(ħc), where a_0 is the Bohr radius, and c the velocity of light. Displacements are in angstroms (Å). Green lines are used for CH_2Cl hydrogen atoms, red lines for CH_2 and the blue one for CH. (B): (*S*)-2-chloromethyl-thiirane. Dependence of the longitudinal and transverse components of the APTs and AATs for the Hydrogen atoms with respect to the CH-bond length (z-direction) (see [12] for the definition of (x,y,z) axes for the CH-bonds). APTs are in atomic unit of charge *e* (electrons), AATs are in units of (ea_0)/(ħc), where a_0 is the Bohr radius, and c the velocity of light. Displacements are in angstroms (Å). Green lines are used for CH_2Cl hydrogen atoms, red lines for CH_2 and the blue one for CH. Figures S7: Graphical representation of three components of hydrogen APT and AAT and their first derivatives with respect to CH bond lengths at equilibrium of the three CH on the ring (z = 0, see ref in the captions of Figure S6). In the top panel, the values of (*R*)-methyloxirane (blue) and (*R*)-methylthiirane (orange) are reported. In the bottom panel, the

values of (*S*)-2-chloromethyl-oxirane (blue) and (*S*)-2-chloromethyl-thiirane (orange) are reported. The *S* configuration is reported to allow a direct comparison with the non-chlorinated systems (see [12]). Figures S8: Fingerprint region between 850 and 1500 cm^{-1} and CH-stretching region. Comparison of experimental IR and VCD spectra with corresponding CCl_4 Boltzmann average computed spectra of (*R*)-chloromethyl thiirane (top two panels) and (*R*)-chloromethyl oxirane (bottom two panels) at the harmonic level and based on GVPT2 approach. Scaling factors of 0.98 and 0.96 were applied to computed harmonic frequencies in the fingerprint and CH-stretching regions respectively. All experimental spectra are in black, computed spectra for (*R*)-chloromethyl thiirane have orange-hue, computed spectra for (*R*)-chloromethyl oxirane have blue-hue. Tables S1: In the top part of the table, energy, enthalpies and free-energy in Hartree units (and relative Boltzmann factors) computed at B3PW91/jun-cc-pVTZ level of theory for chloromethyl thiirane chloromethyl oxirane. In the bottom part, the Boltzmann populations factors taken from Palumbo et al. (https://doi.org/10.1016/j.saa.2020.119061 (accessed on 20 November 2025)) are reported. Tables S2: Comparison of the Calculated Bond Lengths (Å) and Interbond Angle CXC (X = O, S) (deg) for chloromethyl thiirane and chloromethyl oxirane at the B3PW91/jun-cc-pVTZ level of theory. The atom numbering is reported in Figure S5A.

Author Contributions

M.F., G.L., S.A. and S.S.: conceptualization, supervision, writing and editing, reviewing; M.F., G.M., F.L., L.C., C.C. and C.B.: data curation, writing, reviewing; G.M. and B.B.: reviewing; M.F.: software. All authors have read and agreed to the published version of the manuscript.

Funding

This research was funded by the Italian Ministry of University and Research (MUR) through the PRIN 2022 programs: prot. 2022CXHY3A (INVESTCPE) and 2022B3EFJH (SMART HELIX).

Institutional Review Board Statement

Not applicable.

Informed Consent Statement

Not applicable.

Data Availability Statement

The data that support the findings of this study are available on request from the corresponding author.

Acknowledgments

We dedicate this work to Giuseppe Zerbi, the unforgettable mentor of two of us (G.L. and S.A.) during our first research years. The Big & Open Data Innovation Laboratory (BODaI-Lab) of the University of Brescia is acknowledged for providing access to CINECA high-performance computing facilities. The CINECA award under the ISCRA C (CCESTI-HP10CPAAXL) initiative is also acknowledged.

Conflicts of Interest

The authors declare no conflict of interest.

Use of AI and AI-Assisted Technologies

No AI tools were utilized for this paper.

References

1. McGuire, B.A.; Carroll, P.B.; Loomis, R.A.; et al. Discovery of the Interstellar Chiral Molecule Propylene Oxide (CH_3CHCH_2O). *Science* **2016**, *352*, 1449–1452. https://doi.org/10.1126/science.aae0328.
2. Garcia, G.A.; Nahon, L.; Daly, S.; et al. Vibrationally Induced Inversion of Photoelectron Forward-Backward Asymmetry in Chiral Molecule Photoionization by Circularly Polarized Light. *Nat. Commun.* **2013**, *4*, 2132. https://doi.org/10.1038/ncomms3132.
3. Stranges, S.; Turchini, S.; Alagia, M.; et al. Valence Photoionization Dynamics in Circular Dichroism of Chiral Free Molecules: The Methyl-Oxirane. *J. Chem. Phys.* **2005**, *122*, 244307. https://doi.org/10.1063/1.1940632.

4. Turchini, S.; Zema, N.; Contini, G.; et al. Circular Dichroism in Photoelectron Spectroscopy of Free Chiral Molecules: Experiment and Theory on Methyl-Oxirane. *Phys. Rev. A* **2004**, *70*, 014502. https://doi.org/10.1103/physreva.70.014502.
5. Lipparini, F.; Egidi, F.; Cappelli, C.; et al. The Optical Rotation of Methyloxirane in Aqueous Solution: A Never Ending Story? *J. Chem. Theory Comput.* **2013**, *9*, 1880–1884. https://doi.org/10.1021/ct400061z.
6. Nafie, L.A. *Vibrational Optical Activity: Principles and Applications*, 1st ed.; Wiley: Hoboken, NJ, USA, 2011. https://doi.org/10.1002/9781119976516.
7. Šebestík, J.; Bouř, P. Raman Optical Activity of Methyloxirane Gas and Liquid. *J. Phys. Chem. Lett.* **2011**, *2*, 498–502. https://doi.org/10.1021/jz200108v.
8. Polavarapu, P.L. Rotational–Vibrational Circular Dichroism. *Chem. Phys. Lett.* **1989**, *161*, 485–490. https://doi.org/10.1016/0009-2614(89)87025-3.
9. Carnell, M.; Peyerimhoff, S.D.; Breest, A.; et al. Experimental and Quantum-Theoretical Investigation of the Circular Dichroism Spectrum of R-Methyloxirane. *Chem. Phys. Lett.* **1991**, *180*, 477–481. https://doi.org/10.1016/0009-2614(91)85153-N.
10. Breest, A.; Ochmann, P.; Pulm, F.; et al. Experimental Circular Dichroism and VUV Spectra of Substituted Oxiranes and Thiiranes. *Mol. Phys.* **1994**, *82*, 539–551. https://doi.org/10.1080/00268979400100404.
11. Basil, A.; Ben-Tzur, S.; Gedanken, A.; et al. An Extension of the Quadrant Rule in Oxiranes to Non-Alkyl Substituents: The CD of R (−)- and S (+)-Epichlorohydrin. *Chem. Phys. Lett.* **1991**, *180*, 482–484. https://doi.org/10.1016/0009-2614(91)85154-O.
12. Fusè, M.; Longhi, G.; Mazzeo, G.; et al. Anharmonic Aspects in Vibrational Circular Dichroism Spectra from 900 to 9000 Cm^{-1} for Methyloxirane and Methylthiirane. *J. Phys. Chem. A* **2022**, *126*, 6719–6733. https://doi.org/10.1021/acs.jpca.2c05332.
13. Wang, F.; Polavarapu, P.L. Conformational Stability of (+)-Epichlorohydrin. *J. Phys. Chem. A* **2000**, *104*, 6189–6196. https://doi.org/10.1021/jp000757c.
14. Abbate, S.; Longhi, G.; Castiglioni, E. Near-Infrared Vibrational Circular Dichroism: NIR-VCD. In *Comprehensive Chiroptical Spectroscopy*; Berova, N., Polavarapu, P.L., Nakanishi, K., Eds.; Wiley: Hoboken, NJ, USA, 2011; pp 247–273. https://doi.org/10.1002/9781118120187.ch10.
15. Wilson, S.M.; Wiberg, K.B.; Cheeseman, J.R.; et al. Nonresonant Optical Activity of Isolated Organic Molecules. *J. Phys. Chem. A* **2005**, *109*, 11752–11764. https://doi.org/10.1021/jp054283z.
16. Crawford, T.D.; Tam, M.C.; Abrams, M.L. The Problematic Case of (S)-Methylthiirane: Electronic Circular Dichroism Spectra and Optical Rotatory Dispersion. *Mol. Phys.* **2007**, *105*, 2607–2617. https://doi.org/10.1080/00268970701598097.
17. Fusè, M.; Longhi, G.; Mazzeo, G.; et al. The Role of Anharmonicity in the HCD Chromophore in Vibrational Circular Dichroism Spectra and Optical Rotation Data. *J. Phys. Chem. A* **2025,** *129*, 6615–6622. https://doi.org/10.1021/acs.jpca.5c03064.
18. Kleiner, C.M.; Horst, L.; Würtele, C.; et al. Isolation of the Key Intermediates in the Catalyst-Free Conversion of Oxiranes to Thiiranes in Water at Ambient Temperature. *Org. Biomol. Chem.* **2009**, *7*, 1397–1402. https://doi.org/10.1039/b820232j.
19. Polavarapu, P.L.; Hess, B.A.; Schaad, L.J.; et al. Vibrational Spectra of Methylthiirane. *J. Chem. Phys.* **1987**, *86*, 1140–1146. https://doi.org/10.1063/1.452257.
20. Castiglioni, E.; Lebon, F.; Longhi, G.; et al. Vibrational Circular Dichroism in the Near Infrared: Instrumental Developments and Applications. *Enantiomer* **2002**, *7*, 161–173. https://doi.org/10.1080/10242430212877.
21. Frisch, M.J.; Trucks, G.W.; Schlegel, H.B.; et al. *Gaussian 16, Revision C.01*; Gaussian, Inc.: Wallingford, CT, USA, 2019.
22. Bloino, J. A VPT2 Route to Near-Infrared Spectroscopy: The Role of Mechanical and Electrical Anharmonicity. *J. Phys. Chem. A* **2015**, *119*, 5269–5287. https://doi.org/10.1021/jp509985u.
23. Lee, M.J.; Hur, S.W.; Durig, J.R. Conformational Stability, Vibrational Assignments, and Normal Coordinate Analysis from FT-IR Spectra of Xenon Solutions and Ab Initio Calculations of Epichlorohydrin. *J. Mol. Struct.* **1998**, *444*, 99–113. https://doi.org/10.1016/S0022-2860(97)00344-X.
24. Durig, J.R.; Drew, B.R.; Shoop, J.A.; et al. Conformational Stability Determination of Chloromethyl Thiirane from Variable Temperature FT-IR Studies of Rare Gas Solutions, Structural Parameters, and Ab Initio Calculations. *J. Mol. Struct.* **2001**, *569*, 195–212. https://doi.org/10.1016/S0022-2860(01)00430-6.
25. Palumbo, O.; Paolone, A.; Campetella, M.; et al. New Insights into Chloromethyl-Oxirane and Chloromethyl-Thiirane in Liquid and Solid Phase from Low-Temperature Infrared Spectroscopy and Ab Initio Modeling. *Spectrochim. Acta A* **2021**, *247*, 119061. https://doi.org/10.1016/j.saa.2020.119061.
26. Fusè, M.; Mazzeo, G.; Longhi, G.; et al. Ledragna/Lcmodslib: v0.1.2. Available online: https://zenodo.org/records/18155720 (accessed on 20 November 2025)
27. Cahn, R.S.; Ingold, C.; Prelog, V. Specification of Molecular Chirality. *Angew. Chem. Int. Ed.* **1966**, *5*, 385–415. https://doi.org/10.1002/anie.196603851.

28. Fusè, M.; Mazzeo, G.; Bloino, J.; et al. Pushing Measurements and Interpretation of VCD Spectra in the IR, NIR and Visible Ranges to the Detectability and Computational Complexity Limits. *Spectrochim. Acta A* **2024**, *305*, 123496. https://doi.org/10.1016/j.saa.2023.123496.
29. Mendolicchio, M. Harnessing the Power of Curvilinear Internal Coordinates: From Molecular Structure Prediction to Vibrational Spectroscopy. *Theor. Chem. Acc.* **2023**, *142*, 133. https://doi.org/10.1007/s00214-023-03069-7.
30. Mendolicchio, M.; Bloino, J.; Barone, V. Perturb-Then-Diagonalize Vibrational Engine Exploiting Curvilinear Internal Coordinates. *J. Chem. Theory Comput.* **2022**, *18*, 7603–7619. https://doi.org/10.1021/acs.jctc.2c00773.
31. Longhi, G.; Abbate, S.; Zagano, C.; et al. Analysis of the Transition from Normal Modes to Local Modes in a System of Two Harmonically Coupled Morse Oscillators. *Theor. Chim. Acta* **1992**, *82*, 321–337. https://doi.org/10.1007/BF01113262.
32. Abbate, S.; Havel, H.A.; Laux, L.; et al. Vibrational Optical Activity in Deuteriated Phenylethanes. *J. Phys. Chem.* **1988**, *92*, 3302–3311. https://doi.org/10.1021/j100322a045.
33. Bendazzoli, G.L.; Gottarelli, G.; Palmieri, P.; et al. The Optical Activity of R-(+)-Propylene Sulphide. *Mol. Phys.* **1973**, *25*, 473–477. https://doi.org/10.1080/00268977300100421.
34. Gottarelli, G.; Samori, B.; Torre, G. Dynamic-Coupling Approach to the Optical Activity of the 260 Nm Transition of Chiral Thiirans. *J. Chem. Soc. Chem. Commun.* **1974**, 398–399. https://doi.org/10.1039/C39740000398.
35. Moscowitz, A. Some Remarks on the Interpretation of Natural and Magnetically Induced Optical Activity Data. *Proc. R. Soc. Lond. A* **1967**, *297*, 16–26.
36. Mazzeo, G.; Ghidinelli, S.; Ruzziconi, R.; et al. Circularly Polarized Luminescence of Some [2]Paracyclo[2](5,8)quinoliphane Derivatives with Planar and Central Chirality. *ChemPhotoChem* **2022**, *6*, e202100222. https://doi.org/10.1002/cptc.202100222.
37. Moscowitz, A. Theoretical Aspects of Optical Activity Part One: Small Molecules. In *Advances in Chemical Physics*; Prigogine, I., Ed.; Wiley: New York, NY, USA, 1962; Volume 4, pp. 67–112. https://doi.org/10.1002/9780470143506.ch2.
38. Moffitt, W.; Moscowitz, A. Optical Activity in Absorbing Media. *J. Chem. Phys.* **1959**, *30*, 648–660. https://doi.org/10.1063/1.1730025.
39. Brockman, M.W.; Moscowitz, A. Macroscopic Sum Rules in Natural Optical Activity. *Mol. Phys.* **1981**, *43*, 1385–1393. https://doi.org/10.1080/00268978100102141.
40. Polavarapu, P.L. Kramers–Kronig Transformation for Optical Rotatory Dispersion Studies. *J. Phys. Chem. A* **2005**, *109*, 7013–7023. https://doi.org/10.1021/jp0524328.
41. Giorgio, E.; Viglione, R.G.; Zanasi, R.; et al. Ab Initio Calculation of Optical Rotatory Dispersion (ORD) Curves: A Simple and Reliable Approach to the Assignment of the Molecular Absolute Configuration. *J. Am. Chem. Soc.* **2004**, *126*, 12968–12976. https://doi.org/10.1021/ja046875l.
42. Ruud, K.; Taylor, P.R.; Åstrand, P.-O. Zero-Point Vibrational Effects on Optical Rotation. *Chem. Phys. Lett.* **2001**, *337*, 217–223. https://doi.org/10.1016/S0009-2614(01)00187-7.
43. Pedersen, T.B.; Kongsted, J.; Crawford, T.D.; et al. On the Importance of Vibrational Contributions to Small-Angle Optical Rotation: Fluoro-Oxirane in Gas Phase and Solution. *J. Chem. Phys.* **2009**, *130*, 034310. https://doi.org/10.1063/1.3054301.
44. Mort, B.C.; Autschbach, J. Magnitude of Zero-Point Vibrational Corrections to Optical Rotation in Rigid Organic Molecules: A Time-Dependent Density Functional Study. *J. Phys. Chem. A* **2005**, *109*, 8617–8623. https://doi.org/10.1021/jp051685y.
45. Faintich, B.; Parsons, T.; Balduf, T.; et al. Theoretical Study of the Isotope Effect in Optical Rotation. *J. Phys. Chem. A* **2024**, *128*, 8045–8059. https://doi.org/10.1021/acs.jpca.4c03728.
46. Scholten, K.; Engelage, E.; Merten, C. Basis Set Dependence of S=O Stretching Frequencies and Its Consequences for IR and VCD Spectra Predictions. *Phys. Chem. Chem. Phys.* **2020**, *22*, 27979–27986. https://doi.org/10.1039/D0CP05420H.
47. Puente, A.; Chhetri, B.; Kubanek, J.; et al. Revisiting the Absolute Configuration of Peyssonnoside A Using Vibrational Circular Dichroism Spectroscopy. *Symmetry* **2024**, *16*, 133. https://doi.org/10.3390/sym16020133.
48. Mangiavacchi, F.; Mazzeo, G.; Graziani, M.C.; et al. Vibrational and Electronic Circular Dichroism Study of Chiral Seleno Compounds Prepared from a Naphthol Based Diselenide. *Eur. J. Org. Chem.* **2022**, *2022*, e202200282. https://doi.org/10.1002/ejoc.202200282.
49. Ravutsov, M.; Dobrikov, G.M.; Dangalov, M.; et al. 1,2-Disubstituted Planar Chiral Ferrocene Derivatives from Sulfonamide-Directed Ortho-Lithiation: Synthesis, Absolute Configuration, and Chiroptical Properties. *Organometallics* **2021**, *40*, 578–590. https://doi.org/10.1021/acs.organomet.0c00712.
50. Moretti, I.; Torre, G.; Gottarelli, G. The Circular Dichroism and Absolute Configuration of Aryl-Thiiranes. *Tetrahedron Lett.* **1971**, *12*, 4301–4304. https://doi.org/10.1016/S0040-4039(01)97425-8.